Bioactive Materials 3 (2018) 347–354

Contents lists available at ScienceDirect

Bioactive Materials

journal homepage: http://www.keaipublishing.com/en/journals/bioactive-materials/

Doxorubicin-conjugated pH-responsive gold nanorods for combined photothermal therapy and chemotherapy of cancer

Jin Chen [a, 1], Xiao Li [b, c, 1], Xinlian Zhao [a], QianQian Wu [b], Huihui Zhu [b], Zhengwei Mao [a, *], Changyou Gao [a]

[a] MOE Key Laboratory of Macromolecular Synthesis and Functionalization, Department of Polymer Science and Engineering, Zhejiang University, Hangzhou, 310027, PR China
[b] The Department of Gynecologic Oncology, Women's Hospital, School of Medicine, Zhejiang University, Hangzhou, Zhejiang, 310006, China
[c] Women's Reproductive Health Laboratory of Zhejiang Province, Women's Hospital, School of Medicine, Zhejiang University, Hangzhou, Zhejiang, 310006, China

ARTICLE INFO

Article history:
Received 31 October 2017
Received in revised form
5 May 2018
Accepted 7 May 2018

Keywords:
Gold nanorods
Doxorubicin
pH responsive
Photothermal therapy
Combinational therapy

ABSTRACT

Cancer chemotherapy can be hindered by drug resistance which leads to lower drug efficiency. Here, we have developed a drug delivery system that tethers doxorubicin to the surface of gold nanorods via a pH-sensitive linkage (AuNRs@DOX), for a combined photothermal and chemical therapy for cancer. First, AuNRs@DOX is ingested by HepG2 liver cancer cells. After endocytosis, the acidic pH triggers the release of doxorubicin, which leads to chemotherapeutic effects. The gold nanorods are not only carriers of DOX, but also photothermal conversion agents. In the presence of an 808 nm near-infrared laser, AuNRs@DOX significantly enhance the cytotoxicity of doxorubicin via the photothermal effect, which induces elevated apoptosis of hepG2 cancer cells, leading to better therapeutic effects in vitro and in vivo.

1. Introduction

The development of drug resistance is a major obstacle to the success of cancer chemotherapy [1–6]. Developing drug delivery systems using nanotechnology can potentially address this challenge. One possible approach is to inhibit or bypass the P-glycoprotein (P-gp) channel, a membrane-bound active efflux pump which is often overexpressed in the plasma membrane of drug resistant cancer cells. This pump can efflux a broad range of anticancer drugs, so such a strategy might achieve better therapeutic effect [7,8]. For example, it has been shown that certain polymeric carriers can sensitize drug resistant cells to a group of cytotoxic drugs by inhibiting the P-gp drug efflux system [9–11]. Another possible approach is to deliver short interfering RNA (siRNA) that targets the gene encoding P-gp to cancer cells. This would down-regulate P-gp expression and thereby restore intracellular drug levels to the concentrations required for induction of cytotoxicity [12,13].

Combinational therapy has also been acknowledged as a promising strategy to improve therapeutic efficiency. The combination of different drugs and therapeutic modalities may cooperatively suppress cancer development through synergistic effects and reversal of drug resistance [14–22]. Photothermal therapy (PTT) is a rapidly developing cancer phototherapy modality that combines a photosensitizer and a light source. It can effectively induce toxicity to malignant and diseased cells. Near infrared (NIR) laser mediated photothermal therapy in particular has attracted increasing attention for cancer therapy due to its deep tissue penetration and minimal skin/blood absorbance [23–26]. One potential cancer that can be treated with phototherapy is melanoma, a cancer of the skin. Other tumors inside the body require additional equipment, such as optic fiber to guide light into body. Among various NIR photothermal transducers reported thus far, gold nanorods (AuNRs) have been extensively investigated due to their excellent biocompatibility and tunable surface plasmon resonance (SPR) property to convert NIR light into local heat [27,28]. Therefore, we expect advanced anti-cancer efficiency can be achieved by

* Corresponding author.
E-mail address: zwmao@zju.edu.cn (Z. Mao).
Peer review under responsibility of KeAi Communications Co., Ltd.
[1] These authors contribute equally.

https://doi.org/10.1016/j.bioactmat.2018.05.003

combining AuNRs-based PTT and simultaneous application of chemotherapeutic drugs.

There have been several previous investigations of using spherical gold nanoparticles to deliver small chemotherapeutic molecules and large biomacromolecules, including doxorubicin (DOX), small interfering RNA (siRNA), and proteins [19–22]. However, the drugs are usually stably conjugated to the gold nanoparticles, leading to slow release and subsequently reduced toxicity which is unfavorable for the combinational therapy. It would be useful to develop a responsive drug delivery system based on AuNRs with controlled drug release in certain organelles. Wang et al. successfully conjugated DOX to the surface of spherical gold nanoparticles via an acid-labile linkage to overcome multidrug resistance in cancer cells. This represented a combination of highly efficient cellular entry and a responsive intracellular release of DOX from the gold nanoparticles in acidic organelles [29–31]. The photothermal effect may also lead to much faster drug release in tumor cells/tissues, leading to a better tumor therapy effect [16].

Therefore in this study, we conjugated DOX onto the surface of AuNRs with a poly(ethylene glycol) spacer via a pH-responsive linkage (Scheme 1) [29]. This arrangement is favorable for chemotherapy because of its combination of enhanced DOX cellular entry and rapid drug release in acidic organelles. In addition, photothermal therapy was achieved in the presence of 808 nm NIR light to completely ablate cancer cells in vitro and in vivo.

2. Materials and methods

Materials. Doxorubicin hydrochloride was purchased from Zhejiang Hisun Pharmaceutical Co. Ltd., China. α-lipoyl-ω-doxorubicinyl poly(ethylene glycol) with a hydrazone linker (LA-PEG-Hyd-DOX) was synthesized according to literature (Fig. S1) [29]. 3-[4,5-dimethylthiazol-2-yl]-2,5-diphenyltetrazolium bromide (MTT), thiol functionalized mPEG (Mn ~800 D), propidium iodide (PI) and Annexin V-FITC apoptosis detection kit were purchased from Sigma-Aldrich. Milli-Q water was used throughout the experiments. Other common chemicals were of analytical grade and used as received if without specific description.

Preparation of DOX and PEG modified AuNRs. Cetyltrimethylammonium bromide (CTAB) coated AuNRs were prepared according to previous established methods [32]. About 10 mg AuNRs were centrifuged twice at 10,000× g for 15 min to remove free CTAB ligands, and then were incubated in 5 mg/mL thiol PEG or LA-PEG-Hyd-DOX solutions in the presence of 1 mM $NaBH_4$, followed by gentle shaking for 2 days. AuNRs@PEG and AuNRs@DOX were collected by centrifugation (10,000× g for 15 min) and washed five times against water to remove free polymers. The production yields for AuNRs@PEG and AuNRs@DOX from CTAB capped AuNRs are 63.7%wt and 57.6%wt respectively. The loss of AuNRs is mainly happened during centrifugation process after ligand exchange.

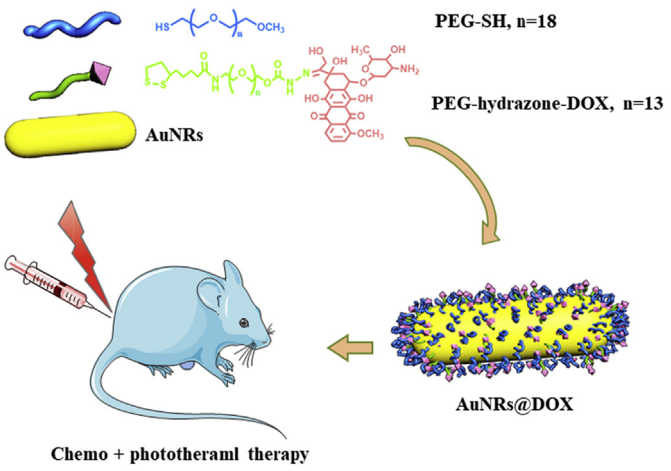

Scheme 1. Schematic illustration to show synthesis of α-lipoyl-ω-doxorubicinyl poly(ethylene glycol) with a hydrazone linker and its application to cap gold nanorods to prepare doxorubicin (DOX) conjugated pH responsive gold nanorods (AuNRs) for cancer therapy.

General characterizations. The AuNRs were observed under transmission electron microscopy (TEM, JEM-1230EX). Hydrodynamic size and zeta potential of the AuNRs were measured by dynamic light scattering (DLS, Zetasizer Nano, Malvern), using a 633 nm He-Ne laser at room temperature. The content of gold was determined using an ICP-MS (Xseries II, Thermo Elemental Corporation, USA).

Release of DOX from DOX-conjugated AuNRs. AuNRs@DOX were incubated in phosphate buffer (PBS, 0.02 M, pH 7.2) or acetate buffer (0.02 M, pH 4.5). The fluorescence emission spectra were recorded at various time intervals. To quantitatively determine the release of DOX, AuNRs@DOX (100 μg/mL) were suspended in PBS or acetate buffer in a dialysis membrane tube (M_W cutoff = 14,000 D, Spectrum Laboratories, USA), and the tube was immersed in 15 mL of PBS or acetate buffer, in a shaking water bath at 37 °C. At predetermined time points, the external buffer was collected and replaced with an equal volume of corresponding buffer. The collected release medium was freeze-dried and dissolved in acetonitrile/water (50/50, v/v), and the concentration of DOX was analyzed by HPLC.

Cell uptake. Human liver carcinoma cell (HepG2) was purchased from Typical Culture Collection of Chinese Academy of Science (Shanghai, China). HepG2 cells were cultured with Dulbecco's modified Eagle medium (DMEM, Gibco), supplemented with 10% FBS, 100 U/mL penicillin, and 100 μg/mL streptomycin. In order to quantify the amount of ingested AuNRs, cells were seeded in a 6-well plate and cultivated to over 80% confluence. The medium was replaced with fresh one containing different AuNRs. After specific time intervals, the cells were carefully washed with PBS to remove the free AuNRs in the medium and the loosely adsorbed ones on the cell surface, and then the cells were harvested by trypsinization [33,34]. The number of cells in each sample was quantified using a Neubauer chamber. The cells were then centrifuged and subsequently dissolved in aqua regia overnight. Finally, samples were diluted 1000 times and measured by ICP-MS to determine the cellular Au content. The cells incubated in particle free medium were used as a control.

In order to track DOX inside cells, HepG2 cells were seeded in 24-well plate at a density of 5×10^4 cell/well and cultured overnight. The cells were incubated with 20 μg/mL AuNRs@DOX for different periods of time. Cells were washed with PBS, stained with lysotracker Green at 37 °C for 15 min, and then observed under confocal laser scanning microscopy (CLSM, TCS SP5, Leica) [39].

Combinational therapy in vitro. Cells were plated in a 96-well plate and incubated overnight for cell adhesion. The medium was replaced with fresh one containing varying concentrations of the AuNRs. After 24 h incubation, the cells were carefully washed with PBS and irradiated using a NIR laser at 808 nm with a beam spot of ~6 mm in diameter at a power of 0.1 W/cm^2 for different time.

After another 24 h incubation, the cell viability was measured using the MTT method [36–38]. The absorbance that has a proportional relationship with the number of living cells and cell viability was recorded at a wavelength of 570 nm by a microplate reader (Model 680, Bio-rad).

The cell apoptosis of HepG2 cells was measured by using a flowcytometry assay based on Annexin V-FITC and PI staining. The cells were incubated with samples for 24 h and irradiated for 1 min.

Subsequently, the cells were stained with Annexin V-FITC/PI for 15 min. Then the cells were collected for flowcytometry analysis. 10000 events were tested in total. Three independent experiments were carried out.

Animals and tumor model. Male BALB/c nude mice (4–6 weeks old) were purchased from the Shanghai Slaccas Animal Company, China. All animal studies were carried out in accordance with the "Guidelines for Animal Experimentation" by the Institutional Animal Care and Use Committee, Zhejiang University. BALB/c nude mice were quarantined for a minimum of 5 days in the SPF grade Animal House under 12 h light/dark cycles at 25 °C with a relative humidity of 50–55%. Tumors were established by subcutaneous (s.c.) injection with HepG2 cells (0.1 mL, 5×10^7/mL) in the back of each nude mouse. After solid tumors developed to about 130 mm^3 in volume, the mice were used for following experiments.

Combinational therapy in vivo. The mice were divided into four groups (six mice in each group) and were intra-tumoral injected with 1) 100 μL physiological saline, 2) 100 μL free DOX solution (4 μg/mL, ~6.9 μM), 3) 100 μL AuNRs@PEG solution (100 μg/mL Au), 4) AuNRs@DOX (100 μg/mL Au and 4 μg/mL DOX). The tumors of mice were irradiated by the 808 nm laser at 0.5 W/cm^2 for 3 min without break. The changes in body weight and tumor volume for each mouse were recorded every three days. The mice were sacrificed at 15 days post therapy. To further detect the therapeutic effect in vivo, tumors were cryosectioned to 3 μm at −20 °C and were allowed to air-dry overnight. The samples were then stained with hematoxylin and eosin (H&E) and observed under a light microscope.

The frozen sections of tumors were fixed in cold acetone for 10 min, air-dried for 30 min, and were treated with 1% H_2O_2 for 10 min at room temperature to eliminate endogenous peroxidases. Samples were rinsed three times (5 min for each time) with PBS, and treated with Powerblock (Biogenex Laboratories, San Ramon, CA) for 6 min to block nonspecific binding. After washed with PBS, the samples were then incubated with antibody against Ki-67 (Abcam, USA) or Hepatocyte Paraffin-1 (HepPar-1, BD Biosciences, CA, USA) for 1 h at 37 °C. After three washes with PBS, the samples were treated with secondary biotinylated anti-rat IgG (1:300, Santa Cruze biotechnology, SC, USA) for 1 h at 37 °C. The slides were washed in PBS and incubated in a 1:50 dilution of avidin-biotinylated enzyme complex (ABC, Vector Laboratories) for 1 h at 37 °C. After three washes with PBS, the samples were treated with

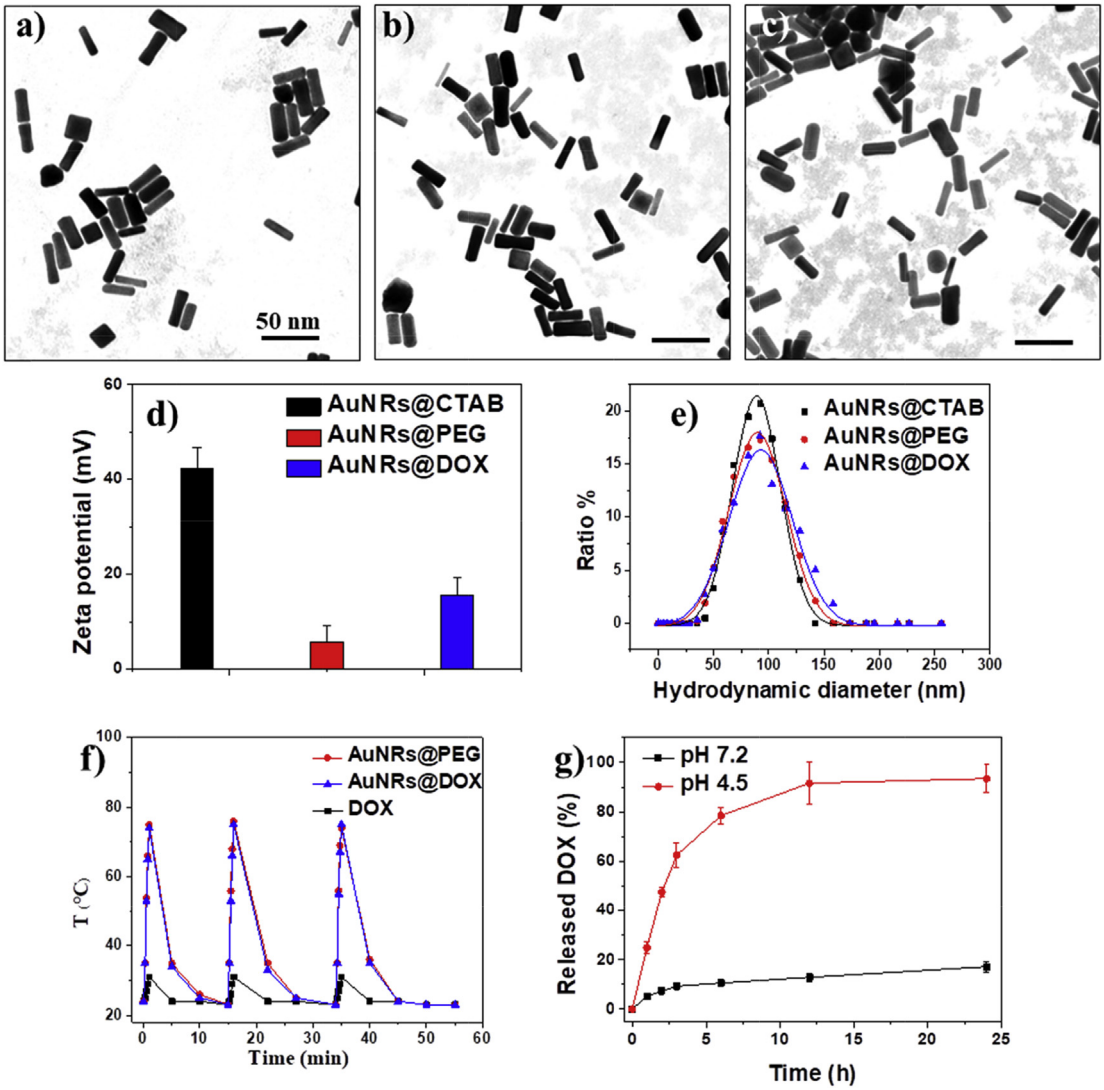

Fig. 1. TEM images of (a) AuNRs@CTAB, (b) AuNRs@PEG, and (c) AuNRs@DOX, respectively. (d) Surface zeta potential and (e) hydrodynamic size of different AuNRs. (f) Plot of temperature of the aqueous dispersions of AuNRs (200 μg/mL) versus irradiation time under 808 nm laser irradiation (0.5 W/cm^2). (g) Quantitative analyses of the in vitro release of doxorubicin at 37 °C from AuNRs@DOX in PBS at pH 7.2 or in acetate buffer at pH 4.5.

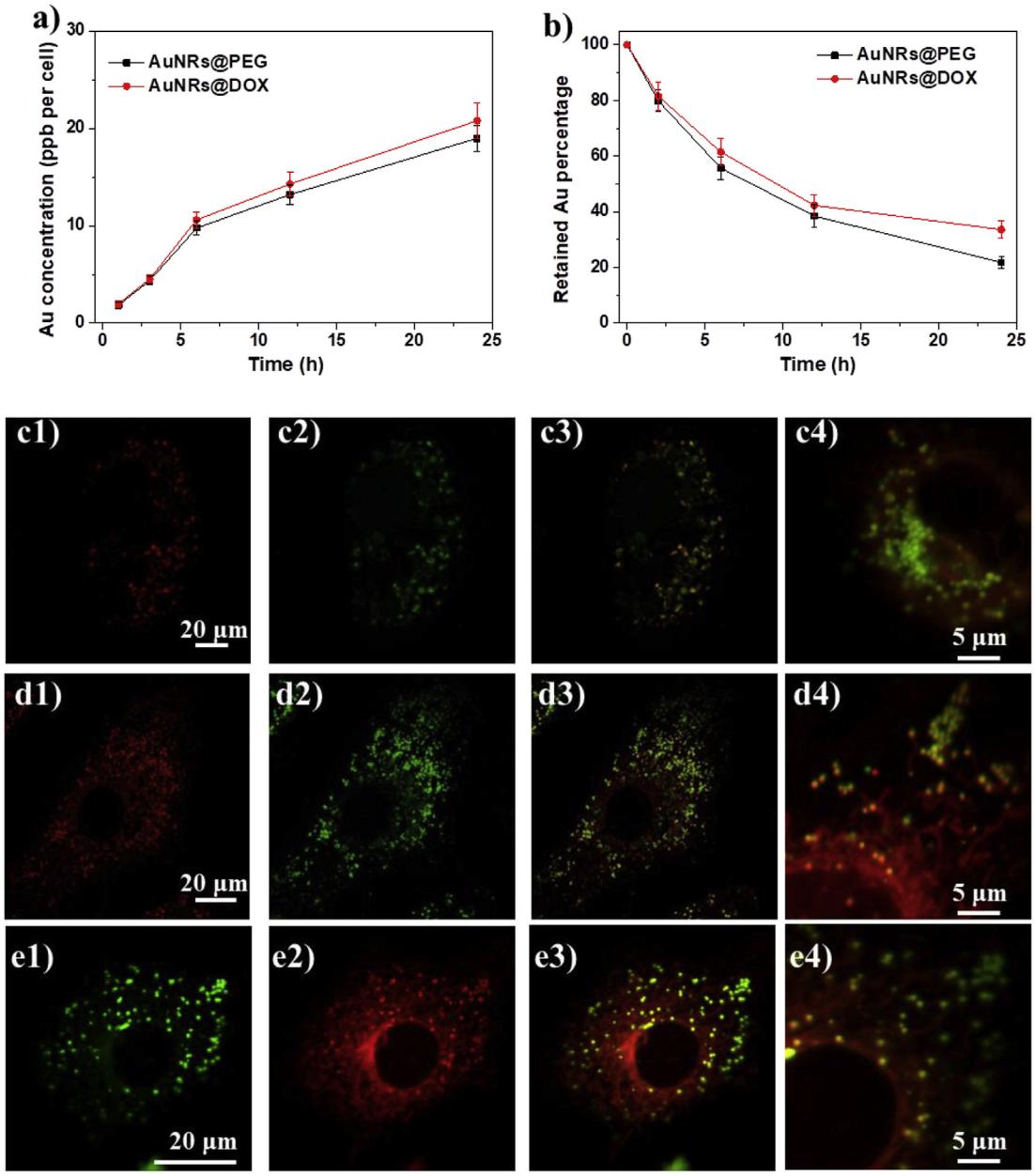

Fig. 2. (a) Plot of the amount of AuNRs ingested by HepG2 cells quantified by ICP-MS versus incubation time. (b) The percentage of the remaining AuNRs in the cells after they are exposed to different AuNRs for 24 h. The feeding concentration of AuNRs is fixed at 20 μg/mL (c–e) Confocal laser microscopic observation of HepG2 cells incubated with AuNRs@DOX for (c) 4 h, (d) 12 h and (e) 24 h. The dose of AuNRs@DOX is 20 μg/mL in the cell culture medium. The cells were counterstained with lysometracker Green for the lysosomes. Column 1: AuNRs@DOX, Column 2: lysosomes, Column 3: merged images, Column 4: Magnified merged images. Scale bars are 20 μm and 5 μm, respectively.

substrate chromogen 3-amino-9-ethylcarbazole (Vector Laboratories) for 30 min. The samples were counterstained in 50% Mayer's hematoxylin and coverslipped in glycerin gelatin [35].

Statistical analysis. Data are reported as mean ± SD. The differences among groups were determined using and unpaired *t*-test (for two groups) and one-way analysis of variance (ANOVA) (for more than two groups) in the Origin software; (*) $p < 0.05$, (**) $p < 0.01$.

3. Results and discussion

3.1. Characterization of obtained AuNRs

As shown in Fig. 1a–c, both AuNRs@PEG and AuNRs@DOX kept original rod-like morphology, with aspect ratio of 4.1 (29 ± 4 nm in length and 7 ± 1 nm in width). The polymer corona cannot be observed under TEM due to low contrast. As shown in Fig. 1d, the surface charge of the AuNRs changed from strongly positive (+40 mV, due to the presence of CTAB) to neutral after PEG modification, which also confirmed the successful surface modification. After introduction of DOX-containing polymer, the surface charge of the AuNRs slightly increased due to positive charge of DOX.

The hydrodynamic diameters obtained from DLS assay of rod-like AuNRs are not precisely reflective of their actual size because the data was calculated based on a spherical model. Nevertheless, they still can be used to demonstrate the tendency of size change of the AuNRs before and after the surface modification. As shown in Fig. 1e, in general the size distribution of AuNRs maintains the same

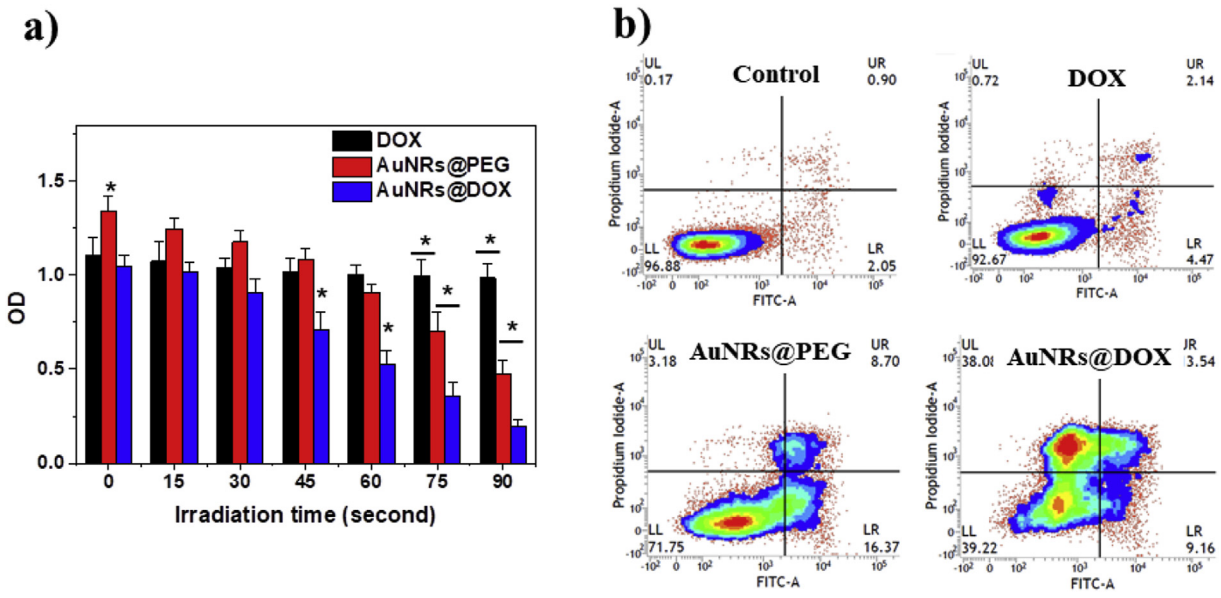

Fig. 3. . (a) Viablity of Cells incubated with free DOX (2 μg/mL, ~3.5 μM, corresponding to the DOX content of 50 μg/mL AuNRs@DOX) and different AuNRs (50 μg/mL) for 24 h, and then irradiated under a 808 nm NIR laser (0.1 W/cm^2) for different period. * indicates significant difference between different groups within same time frame at $p < 0.05$ level. (b) Apoptosis analysis of cells treated with DOX and different AuNRs (50 μg/mL) and irradiated with an 808 nm NIR laser for 90 s (0.1 W/cm^2).

Table 1
Summarized cell apoptosis results.

Sample	Vital cells (%)	Early apoptotic cells (%)	Late apoptotic/Necrotic cells (%)	Dead cells (%)
Control	95.7 ± 1.2	1.9 ± 0.2	0.8 ± 0.2	0.8 ± 0.3
DOX	92.5 ± 1.9	4.8 ± 0.6	2.2 ± 0.5	0.9 ± 0.2
AuNRs@PEG + L	70.2 ± 2.8	16.9 ± 1.3	8.5 ± 0.9	3.5 ± 0.6
AuNRs@DOX + L	39.8 ± 3.2	9.5 ± 0.7	3.9 ± 0.4	38.1 ± 2.8

with a single peak after surface modification, suggesting good colloidal stability of obtained AuNRs. The sizes of AuNRs@PEG and AuNRs@DOX increased slightly after surface modification, possibly due to the relatively larger hydrodynamic size of hydrophilic polymers than small molecular CTAB.

The amount of LA-PEG-Hyd-DOX conjugated to the AuNRs was 9.1 ± 1.1% by weight ratio (LA-PEG-Hyd-DOX to AuNRs@DOX), calculated from the results of remaining LA-PEG-Hyd-DOX in the supernatant of the reaction mixture after centrifugation. The results indicated that AuNRs@DOX contained about 4% DOX molecules by weight ratio. Due to thermal gravimetric analysis, the total polymer contributed 14.6 ± 1.7% by weight ratio of AuNRs@DOX. Therefore PEG contributed about 5.5% by weight ratio of AuNRs@-DOX, providing good colloidal stability of the nanorods.

The obtained AuNRs@PEG and AuNRs@DOX both have excellent photothermal transfer ability, as evidenced by the rapid temperature increase as high as 75 °C under an 808 nm laser irradiation within 1 min, with a concentration of AuNRs at 200 μg/mL (Fig. 1f). In contrast, the DOX solution received the same laser irradiation remains cool, confirming the light-heat transition was contributed by the AuNRs.

Although we do not have a suitable method to directly observe the cleavage of chemical bonds on AuNRs, the degradation of hydrazone bonds of AuNRs@DOX will result in the release of doxorubicin from the nanorods. The amount of released DOX at predetermined time intervals under different pH environment was measured. As shown in Fig. 1g, about 17% of the total doxorubicin from AuNRs@DOX was released from the carrier after 24 h of incubation at pH 7.4. However, a much faster release of doxorubicin was observed when AuNRs@DOX were incubated at pH 4.5, reaching over 90% of cumulative release of conjugated drug after 24 h. The results suggested that the cleavage of hydrazone linkers was accelerated at lower pH value.

3.2. Cell uptake of AuNRs

Both AuNRs@PEG and AuNRs@DOX can be ingested by human hepatocellular carcinoma (HepG2) cells (Fig. 2a). The gold content in cells increased gradually along with incubation time without obivious toxicity, due to low DOX concentration in the system. Both AuNRs showed similar cell uptake and removal tendency in HepG2 cells (Fig. 2a and b), possibly due to the similar surface property with hydrophilic PEG molecules.

The intracellular distribution of AuNRs@DOX was also studied by taking advantage of the autofluorescence of DOX. After 4 h incubation, a lot of AuNRs were ingested by cells and localized within lysosomes (Fig. 2c). Only a small fraction of DOX was released out of the lysosomes. After 12 h and 24 h incubation, more and more DOX were released out of the lysosomes, suggesting the pH triggered release of DOX molecules (Fig. 2d and e). A certain fraction of AuNRs@DOX was always trapped in the lysosomes, possibly due to limited diffusion of free DOX from lysosomes and/or incomplete degradation of hydrazone bonds because the process consumes H^+ and may lead to increase of the pH in the lysosomes.

3.3. Cytotoxicity in vitro

The viability of HepG2 cells that received different treatment

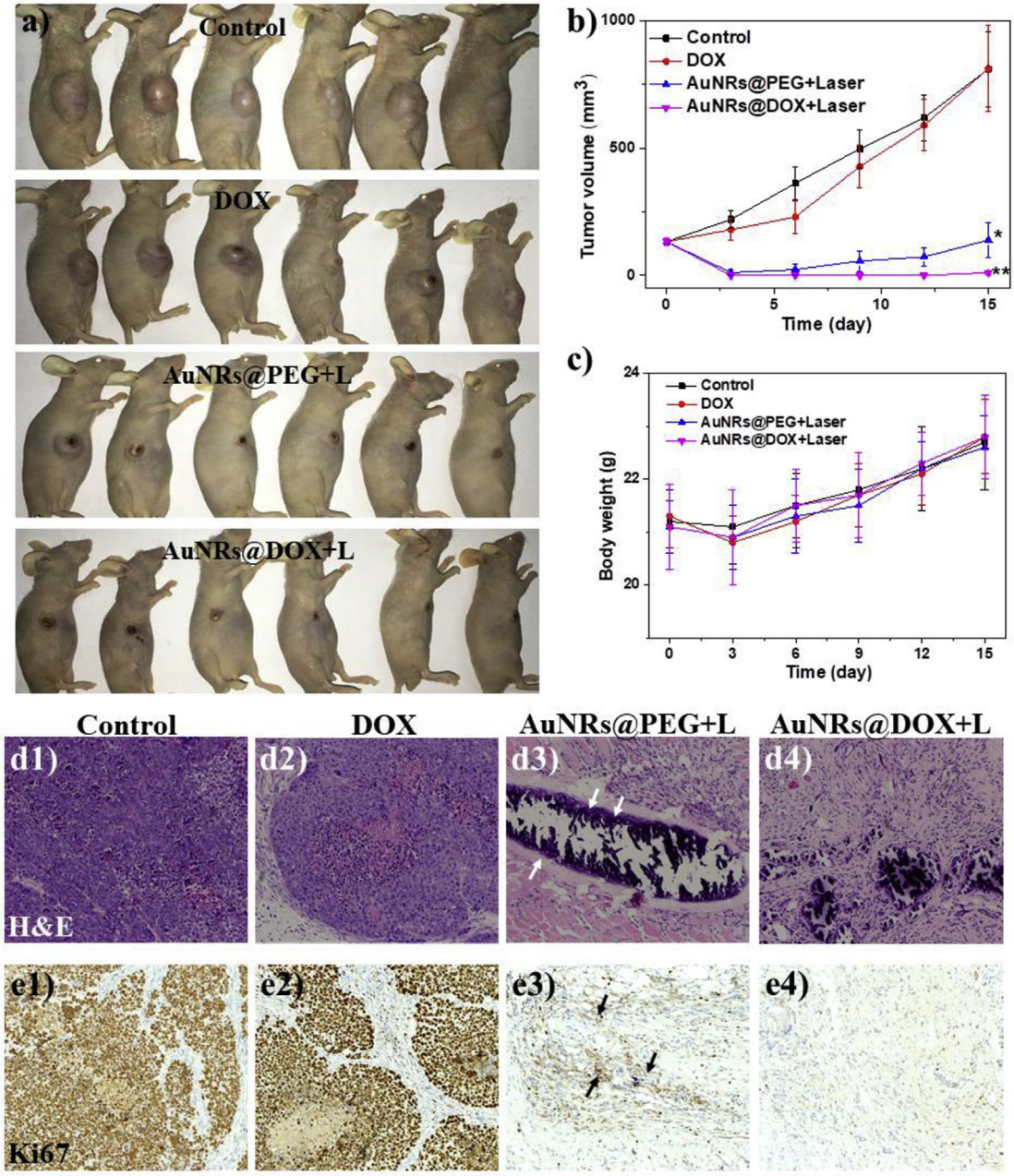

Fig. 4. Digital images of tumor bearing mice treated with DOX (4 μg/mL, ~6.9 μM, corresponding to the DOX content of 100 μg/mL AuNRs@DOX) and different AuNRs (100 μg/mL) together with 3 min laser irradiation at 808 nm (0.5 W/cm^2). Each tumor received 100 μL solutions by intra-tumoral injection. (b) Average tumor volume and (c) body weight of the mice in different groups. * and ** indicate significant difference at $p < 0.05$ and $p < 0.01$ level, respectively. (d) H&E and (e) Ki67 analyses of tumor tissues after various treatments. Column 1: untreated control, Column 2: free DOX, Column 3: AuNRs@PEG with laser irradiation, Column 4: AuNRs@DOX with laser irradiation. The images were amplified for 100 times.

was quantitatively analyzed by MTT assay. As shown in Fig. 3a, cells treated with free DOX demonstrated about 80% of the viability compared to untreated control. There is no significant difference of viability between the cells treated with free DOX and those irradiated for different time. Therefore, we can reasonably conclude that the laser itself has no ability to kill cells at such a low power density. The cells treated with AuNRs@DOX showed similar viability without laser irradiation. Wang et al. reported enhanced toxicity of conjugated DOX on gold nanoparticles for drug-resistant cancer cells [14]. But in our study, we did not observe this effect. This might be attributed to the higher sensitivity of our HepG2 cells to DOX, which could reduce the difference between free drug and conjugated drug. In contrast, AuNRs@PEG had negligible influence on viability of HepG2 cells without laser irradiation. After applying laser irradiation, both AuNRs@PEG and AuNRs@DOX demonstrated stronger impedance on cell viability with irradiation time due to the photothermal effect. The AuNRs@DOX always had significantly higher toxicity to cells compared to AuNRs@PEG and DOX, demonstrating the combinational therapeutic ability for cancer cells. Similar cytotoxicity was observed in doxorubicin resistant MCF-7/ADR cells (Fig. S3), suggesting the potential application of combined therapy to drug resistant cancer.

In order to further distinguish the cells at different apoptosis/necrosis stages, the cells were examined with dual fluorescence of

Annexin V-FITC/PI by flowcytometry. As shown in Fig. 3b and Table 1, UL represents dead cells, which were negative for Annexin V-FITC and positive for PI. UR represents late apoptosis or necrosis cells, which were positive for both Annexin V-FITC and PI. LR represents early apoptosis cells, which were positive for Annexin V-FITC and negative for PI. LL represented vital cells, which was negative for both Annexin V-FITC and PI. The populations of apoptosis and dead cells were >60% immediately after treatment with AuNRs@DOX + laser irradiation (Table 1), confirming the combinational therapeutic effect. The populations of apoptotic and dead cells were about 30% after the cells were treated with AuNRs@PEG + laser irradiation, indicating that the photothermal effect alone was not enough to immediately kill all cancer cells. In contrast, only 8% of the cells were identified as apoptosis or dead when they were treated with free DOX.

3.4. Chemo and photothermal treatment of xenograft tumor in vivo

The in vivo therapy study was carried out in HepG2 tumor bearing mice. After treatment for 15 d, the digital photos of mice in different groups were taken to visually display the therapy effect (Fig. 4a). The therapeutic effect was also evaluated by monitoring the tumor volume every three days (Fig. 4b). The tumors that received DOX injection slightly shrank after 3 days and then regrew again, finally reaching a similar volume to that of control. The results indicated unsatisfactory effect of free DOX, mainly due to its extremely low dosage. In previous studies, we have demonstrated that light irradiation only and AuNRs@PEG without light irradiation have no effect on tumor growth [28]. After treatment with AuNRs@PEG and laser irradiation for 3 min (808 nm, 0.5 W/cm^2), the tumors were heated to about 56 °C on the surface. The tumors were almost completely destroyed after treatment but recurred again after 9 days, illustrating an unsatisfactory photothermal therapy effect. This is because the localized heat is not enough to completely destroy the whole tumor. For the group treated with AuNRs@DOX for 3 min (also heated to about 56 °C on the surface), most of the mice were completely healed without tumor recurrence within 60 days (n = 6, Fig. S4) on all mice, indicating the excellent combinational therapeutic effect of chemo and photothermal therapy, validating the potential application of this responsive dual modality therapeutic agent for cancer therapy.

The results were also confirmed by H&E staining (Fig. 4d) and Ki67 staining (Fig. 4e, viable tumor cells are brown). Obviously, a huge area of tumor cells was observed in the control group (Column 1) and in the free DOX group (Column 2). In the group treated with AuNRs@PEG + laser irradiation (Column 3), the majority of tumor cells were ablated. But there are a few tumor cells remaining (indicated by arrow), which were responsible for the recurrence. In particular, no tumor cells were found in the group treated with AuNRs@DOX + laser irradiation (Column 4), which demonstrated the most effective combinational therapy.

In summary, the developed DOX-conjugated pH-responsive AuNRs have several advantages: 1) the AuNRs are biocompatible and robust nanomaterials could be conveniently prepared by simple wet chemistry; 2) the pH-responsive DOX conjugated polymer enables the feasible loading of drug onto the AuNRs and rapid release of toxic drug under acidic environment inside cancer cells; 3) the modification of AuNRs together with PEG and drug-conjugated polymer is simple and effective, with tunable drug loading ability and capacity for cost-effective scale up preparation. In the resulting AuNRs@DOX complex nanomaterials, AuNRs could efficiently convert non-thermal NIR light into local heat and ablate majority heat intolerant cancer cells. DOX payload, on the other hand, could inhibit the proliferation of residual cancer cells owing to its severe cytotoxicity. In this study, a simple sub-cutaneous cancer model on mouse was used to confirm that AuNRs@DOX treatment in combination with NIR laser irradiation could completely inhibit the growth of tumor in vivo, implying a synergistically therapeutic outcome between chemotherapy and photothermal therapy. Limited by positive surface charge of AuNRs@DOX, feasablility for i.v. injection is unlikely because of lung clearance. The AuNRs with maximum SPR peak at 808 nm may not suitable for clinical application because of limited tissue penetration of the light. Further optimization of the system may be achieved by using nanoparticles with a maximum SPR peak in the second NIR window. This will in turn lead to better tissue penetration of the light as well as better surface decoration, enabling lasting circulation in blood and improved tumor targeting.

4. Conclusions

A dual modality therapeutic nanoplatform based on DOX-conjugated pH-responsive AuNRs was developed for cancer therapy. The AuNRs@DOX nanoparticles could induce cell apoptosis more efficiently with the presence of an NIR laser than free DOX and AuNRs@PEG + laser irradiation, indicating the excellent combinational therapeutic effect in vitro and in vivo. These results imply promising potentials of AuNRs@DOX mediated combination of photothermal therapy and chemotherapy against cancers.

Acknowledgements

The authors thank Mr. Liangjie Hong for the help of animal experiments. The authors are grateful to the financial support from the National Key Research and Development Program of China (2016YFB0700804), the National Natural Science Foundation of China (51673171), Zhejiang Provincial Natural Science Foundation of China (LR16E030001, LR15H160001), and the Fundamental Research Funds for the Central Universities of China (2018QNA4057). This study is supported in part by Key Laboratory of Reproductive Genetics (Zhejiang University), Ministry of Education, P. R. China/Women's Reproductive Health Key Laboratory of Zhejiang Province/Uterine Tumors Research Center of Zhejiang Province (ZDFY2017-RG/RH-001).

Appendix A. Supplementary data

Supplementary data related to this article can be found at https://doi.org/10.1016/j.bioactmat.2018.05.003.

References

[1] R.A. Petros, J.M. DeSimone, Strategies in the design of nanoparticles for therapeutic applications, Nat. Rev. Drug Discov. 9 (8) (2010) 615–627.
[2] Z. Ge, S. Liu, Functional block copolymer assemblies responsive to tumor and intracellular microenvironments for site-specific drug delivery and enhanced imaging performance, Chem. Soc. Rev. 42 (17) (2013) 7289–7325.
[3] V.P. Torchilin, Multifunctional, stimuli-sensitive nanoparticulate systems for drug delivery, Nat. Rev. Drug Discov. 13 (11) (2014) 813–827.
[4] E.K. Lim, T. Kim, S. Paik, S. Haam, Y.M. Huh, K. Lee, Nanomaterials for theranostics: recent advances and future challenges, Chem. Rev. 115 (1) (2015) 327–394.
[5] H. Chen, W. Zhang, G. Zhu, J. Xie, X. Chen, Rethinking cancer nanotheranostics, Nature Reviews Materials 2 (7) (2017).
[6] G. Yu, T.R. Cook, Y. Li, X. Yan, D. Wu, L. Shao, J. Shen, G. Tang, F. Huang, X. Chen, P.J. Stang, Tetraphenylethene-based highly emissive metallacage as a component of theranostic supramolecular nanoparticles, Proc. Natl. Acad. Sci. U. S. A 113 (48) (2016) 13720–13725.
[7] D. Peer, J.M. Karp, S. Hong, O.C. FaroKhzad, R. Margalit, R. Langer, Nanocarriers as an emerging platform for cancer therapy, Nat. Nanotechnol. 2 (12) (2007) 751–760.
[8] H.X. Wang, Z.Q. Zuo, J.Z. Du, Y.C. Wang, R. Sun, Z.T. Cao, X.D. Ye, J.L. Wang, K.W. Leong, J. Wang, Surface charge critically affects tumor penetration and therapeutic efficacy of cancer nanomedicines, Nano Today 11 (2) (2016) 133–144.

[9] E.V. Batrakova, S. Li, A.M. Brynskikh, A.K. Sharma, Y. Li, M. Boska, N. Gong, R.L. Mosley, V.Y. Alakhov, H.E. Gendelman, A.V. Kabanov, Effects of pluronic and doxorubicin on drug uptake, cellular metabolism, apoptosis and tumor inhibition in animal models of MDR cancers, J. Contr. Release 143 (3) (2010) 290–301.
[10] D. Wang, Z. Xu, H. Yu, X. Chen, B. Feng, Z. Cui, B. Lin, Q. Yin, Z. Zhang, C. Chen, J. Wang, W. Zhang, Y. Li, Treatment of metastatic breast cancer by combination of chemotherapy and photothermal ablation using doxorubicin-loaded DNA wrapped gold nanorods, Biomaterials 35 (29) (2014) 8374–8384.
[11] Z.T. Cao, Z.Y. Chen, C.Y. Sun, H.J. Li, H.X. Wang, Q.Q. Cheng, Z.Q. Zuo, J.L. Wang, Y.Z. Liu, Y.C. Wang, J. Wang, Overcoming tumor resistance to cisplatin by cationic lipid-assisted prodrug nanoparticles, Biomaterials 94 (2016) 9–19.
[12] Z.J. Deng, S.W. Morton, E. Ben-Akiva, E.C. Dreaden, K.E. Shopsowitz, P.T. Hammond, Layer-by-layer nanoparticles for systemic codelivery of an anticancer drug and siRNA for potential triple-negative breast cancer treatment, ACS Nano 7 (11) (2013) 9571–9584.
[13] C.F. Xu, H.B. Zhang, C.Y. Sun, Y. Liu, S. Shen, X.Z. Yang, Y.H. Zhu, J. Wang, Tumor acidity-sensitive linkage-bridged block copolymer for therapeutic siRNA delivery, Biomaterials 88 (2016) 48–59.
[14] G. Yu, B. Yung, Z. Zhou, Z.W. Mao, X. Chen, Artificial molecular machines in nanotheranostics, ACS Nano 12 (2018) 7–12.
[15] W. Fan, B. Yung, P. Huang, X. Chen, Nanotechnology for multimodal synergistic cancer therapy, Chem. Rev. 117 (22) (2017) 13566–13638.
[16] G. Yu, Z. Yang, X. Fu, B. Yung, J. Yang, Z.W. Mao, L. Shao, B. Hua, Y. Liu, F. Zhang, Q. Fan, O. Jacobson, A. Jin, C. Gao, F. Huang, X. Chen, Polyrotaxane-based supramolecular theranostics, Nat. Commun. 9 (2018) 766.
[17] G. Yu, M. Zhang, M. Saha, Z.W. Mao, J. Chen, Y. Yao, Z. Zhou, Y. Liu, C. Gao, F. Huang, X. Chen, P. Stang, Antitumor activity of a unique polymer that incorporates a fluorescent self-assembled metallacycle, J. Am. Chem. Soc. 139 (2017) 15940–15949.
[18] Z. Zhang, L. Wang, J. Wang, X. Jiang, X. Li, Z. Hu, Y. Ji, X. Wu, C. Chen, Mesoporous Silica-Coated Gold Nanorods as a Light-mediated multifunctional theranostic platform for cancer treatment, Adv. Mater. 24 (11) (2012) 1418–1423.
[19] S. Shen, H. Tang, X. Zhang, J. Ren, Z. Pang, D. Wang, H. Gao, Y. Qian, X. Jiang, W. Yang, Targeting mesoporous silica-encapsulated gold nanorods for chemo-photothermal therapy with near-infrared radiation, Biomaterials 34 (12) (2013) 3150–3158.
[20] F. Ren, S. Bhana, D.D. Norman, J. Johnson, L. Xu, D.L. Baker, A.L. Parrill, X. Huang, Gold nanorods carrying paclitaxel for photothermal-chemotherapy of cancer, Bioconjugate Chem. 24 (3) (2013) 376–386.
[21] D. Wang, Z. Xu, H. Yu, X. Chen, B. Feng, Z. Cui, B. Lin, Q. Yin, Z. Zhang, C. Chen, J. Wang, W. Zhang, Y. Li, Treatment of metastatic breast cancer by combination of chemotherapy and photothermal ablation using doxorubicin-loaded DNA wrapped gold nanorods, Biomaterials 35 (29) (2014) 8374–8384.
[22] X. Li, M. Takashima, E. Yuba, A. Harada, K. Kono, PEGylated PAMAM dendrimer-doxorubicin conjugate-hybridized gold nanorod for combined photothermal-chemotherapy, Biomaterials 35 (24) (2014) 6576–6584.
[23] K. Welsher, S.P. Sherlock, H. Dai, Deep-tissue anatomical imaging of mice using carbon nanotube fluorophores in the second near-infrared window, Proc. Natl. Acad. Sci. U. S. A 108 (22) (2011) 8943–8948.
[24] A. Kumar, S. Kim, J.-M. Nam, Plasmonically engineered nanoprobes for biomedical applications, J. Am. Chem. Soc. 138 (44) (2016) 14509–14525.
[25] L. Cheng, C. Wang, L. Feng, K. Yang, Z. Liu, Functional nanomaterials for phototherapies of cancer, Chem. Rev. 114 (21) (2014) 10869–10939.
[26] R. Vankayala, C.C. Lin, P. Kalluru, C.S. Chiang, K.C. Hwang, Gold nanoshells-mediated bimodal photodynamic and photothermal cancer treatment using ultra-low doses of near infra-red light, Biomaterials 35 (21) (2014) 5527–5538.
[27] C. Grabinski, N. Schaeublin, A. Wijaya, H. D'Couto, S.H. Baxamusa, K. Hamad-Schifferli, S.M. Hussain, Effect of gold nanorod surface chemistry on cellular response, ACS Nano 5 (4) (2011) 2870–2879.
[28] G. Sheng, Y. Chen, L. Han, Y. Huang, X. Liu, L. Li, Z. Mao, Encapsulation of indocyanine green into cell membrane capsules for photothermal cancer therapy, Acta Biomater. 43 (2016) 251–261.
[29] F. Wang, Y.C. Wang, S. Dou, M.H. Xiong, T.M. Sun, J. Wang, Doxorubicin-tethered responsive gold nanoparticles facilitate intracellular drug delivery for overcoming multidrug resistance in cancer cells, ACS Nano 5 (5) (2011) 3679–3692.
[30] T.M. Sun, Y.C. Wang, F. Wang, J.Z. Du, C.Q. Mao, C.Y. Sun, R.Z. Tang, Y. Liu, J. Zhu, Y.H. Zhu, X.Z. Yang, J. Wang, Cancer stem cell therapy using doxorubicin conjugated to gold nanoparticles via hydrazone bonds, Biomaterials 35 (2) (2014) 836–845.
[31] H. Park, H. Tsutsumi, H. Mihara, Cell-selective intracellular drug delivery using doxorubicin and alpha-helical peptides conjugated to gold nanoparticles, Biomaterials 35 (10) (2014) 3480–3487.
[32] H. Zhu, Y. Chen, F.J. Yan, J. Chen, X.F. Tao, J. Ling, B. Yang, Q.J. He, Z.W. Mao, Polysarcosine brush stabilized gold nanorods for in vivo near-infrared photothermal tumor therapy, Acta Biomater. 50 (2017) 534–545.
[33] X. Zhou, M. Dorn, J. Vogt, D. Spemann, W. Yu, Z. Mao, I. Estrela-Lopis, E. Donath, C. Gao, A quantitative study of the intracellular concentration of graphene/noble metal nanoparticle composites and their cytotoxicity, Nanoscale 6 (15) (2014) 8535–8542.
[34] P. Jiang, Y. Zhang, C. Zhu, W. Zhang, Z. Mao, C. Gao, Fe_3O_4/BSA particles induce osteogenic differentiation of mesenchymal stem cells under static magnetic field, Acta Biomater. 46 (2016) 141–150.
[35] L.H. Peng, Y.F. Huang, C.Z. Zhang, J. Niu, Y. Chen, Y. Chu, Z.H. Jiang, J.Q. Gao, Z.W. Mao, Integration of antimicrobial peptides with gold nanoparticles as unique non-viral vectors for gene delivery to mesenchymal stem cells with antibacterial activity, Biomaterials 103 (2016) 137–149.
[36] T. Ren, S. Yu, Z. Mao, C. Gao, A complementary density gradient of zwitterionic polymer brushes and NCAM peptides for selectively controlling directional migration of Schwann cells, Biomaterials 56 (2015) 58–67.
[37] P. Jiang, Z. Mao, C. Gao, Combinational effect of matrix elasticity and alendronate density on differentiation of rat mesenchymal stem cells, Acta Biomater. 19 (2015) 76–84.
[38] W. Zhang, P. Jiang, Y. Chen, P. Luo, G. Li, B. Zheng, W. Chen, Z. Mao, C. Gao, Suppressing the cytotoxicity of CuO nanoparticles by uptake of curcumin/BSA particles, Nanoscale 8 (18) (2016) 9572–9582.
[39] L.H. Peng, Y.H. Zhang, L.J. Han, C.Z. Zhang, J.H. Wu, X.R. Wang, J.Q. Gao, Z.W. Mao, Cell membrane capsules for encapsulation of chemotherapeutic and cancer cell tTargeting in vivo, ACS Appl. Mater. Interfaces 7 (33) (2015) 18628–18637.